EFDA–JET–PR(09)20

P. Maget, H. Lütjens, R. Coelho, B. Alper, M. Brix, P. Buratti, R.J. Buttery,
E. De la Luna, N. Hawkes, I. Jenkins, C. Challis, C. Giroud, X. Litaudon,
J. Mailloux, M. Ottaviani and JET EFDA contributors

Modelling of (2,1) NTM Threshold in JET Advanced Scenarios

Modelling of (2,1) NTM Threshold in JET Advanced Scenarios

P. Maget[1], H. Lütjens[2], R. Coelho[3], B. Alper[4], M. Brix[4], P. Buratti[5], R.J. Buttery[4], E. De la Luna[6], N. Hawkes[4], I. Jenkins[4], C. Challis[4], C. Giroud[4], X. Litaudon[1], J. Mailloux[4], M. Ottaviani[1] and JET EFDA contributors*

JET-EFDA, Culham Science Centre, OX14 3DB, Abingdon, UK

[1]CEA, IRFM, F-13108 Saint Paul-lez-Durance, France
[2]Centre de Physique Th´eorique, Ecole Polytechnique, CNRS, France
[3]Inst Plasmas & Fusao Nucl, EURATOM Assoc, IST, P-1049001 Lisbon, Portugal
[4]EURATOM-UKAEA Fusion Association, Culham Science Centre, OX14 3DB, Abingdon, OXON, UK
[5]ENEA Fus, EURATOM Assoc, I-00040 Frascati, Italy
[6]Laboratorio Nacional de Fusión, Asociación EURATOM-CIEMAT, Madrid, Spain
** See annex of F. Romanelli et al, "Overview of JET Results",*
(Proc. 22 [nd] IAEA Fusion Energy Conference, Geneva, Switzerland (2008)).

Preprint of Paper to be submitted for publication in
Nuclear Fusion

ABSTRACT.
The limit to high performances advanced scenario discharges with q_{min} above unity is generally set by the (2,1) MHD mode in JET. We investigate here the possibility that this mode is a (2,1) Neoclassical Tearing Mode (NTM) by computing the critical island width at which such mode would be unstable, using a non linear Magneto-Hydro-Dynamic (MHD) code where the relevant bootstrap current physics is accounted for. We show that the triggering of a (2,1) NTM is consistent with a lowering of the critical island width as the plasma current diffuses towards the centre. This is explained partly by the increase of the magnetic shear at the resonant surface, which weakens the curvature stabilisation term, as found in the analytical framework of a Generalized Rutherford Equation. A comparison with experiment is made in the non linear regime, showing encouraging results on the dynamics of the confinement degradation and mode structure.

1. INTRODUCTION

The exploration of high performance limits in present tokamak plasma discharges allows determining some optimum conditions under which ideal as well as resistive Magneto-Hydro-Dynamic (MHD) modes can be avoided. The triggering of resistive instabilities below the ideal MHD limit has long been observed to be the main obstacle to the achievement of good performance, even though the consequence could be limited to a degradation of the core confinement, without disruption. Experiments exploring the operational domain in the normalized beta β_N ($\beta_N = \beta aB/I_p^{MA}$, with $\beta = 2\mu_0 \langle p \rangle / B^2$, $\langle p \rangle$ is the volume average plasma pressure, a is the plasma minor radius, B is the magnetic field on axis, I_p^{MA} is the total plasma current expressed in MA) have found this so called soft β limit (in contrast to disruptive ones) on TFTR [1], JET [2], DIII-D [3], JT60 [4], COMPASS-D [5], T10 [6], TCV [7] or TEXTOR [8]. In these plasma with high pressure, the drive for island growth is dominated by a non linear coupling between the pressure and the parallel current density, through the bootstrap current (driven by the pressure gradient), resulting in the emergence of a metastable branch called Neoclassical Tearing Mode (NTM) [9]. Extrapolating the condition of existence of these modes to large tokamak devices as ITER stimulates broad interest in the fusion community, in the prospect of determining scaling laws for the critical island width or for the β limit above which they are triggered [10].

In the present work, we model the threshold and dynamics of NTMs in high-β_N discharges on JET, where the current profile is optimized for maximizing the boostrap fraction, as foreseen in an Advanced Tokamak scenario [11]. The performance of these discharges is limited by the triggering of a n = 1 mode mainly localised at the q = 2 surface, where q is the safety factor ($q = d\Phi/d\Psi$ with Φ and Ψ the toroidal and poloidal magnetic fluxes respectively), and n is the toroidal mode number [12, 13]. The mode evolves to a large island on q = 2, with significant confinement degradation (~15% in the H_{89} confinement scaling factor for the example we have modelled), thus motivating investigations about its nature as well as about possible ways to avoid its appearance. In complement to database analysis, modelling focussed on few specific discharges has been initiated, as reported

in the present paper. Our goal for this work was to determine the threshold for metastable resistive modes with a full MHD non linear code covering the standard one fluid MHD model with simplified description of the bootstrap current effect [14], and to check if the appearance of the (m = 2, n = 1) mode was consistent with the evolution of the critical island width (m is the poloidal mode number). Also, the dynamics of the confinement degradation produced by the mode can be compared with the experiment, thus providing a verification of our ability to model the impact of NTMs.

The modelling of NTM threshold and dynamics has long been performed in the analytical framework developed by Rutherford [15], where the boostrap current contribution and heat transport effects [16], toroidal curvature effect [17, 18], and polarization effect [19, 20] have been added. Such developments have been used to model NTM observations in many tokamaks, and they allowed deriving scaling laws [21] and improving our understanding of the physics at play [22]. Non linear simulations using a full description of the magnetic and velocity fields (in contrast with simplified treatments using scalar potentials) have been performed on ITER reference equilibria [23, 24, 25], allowing a comparison with the predictions of a Generalized Rutherford Equation for the critical and the saturated island widths, and suggesting significant discrepancies. In these works, the seeding process of the NTM has not been considered, and the seed is imposed as an initial condition for the non linear evolution. Indeed, although several seeding mechanisms could be relevant for the standard one fluid MHD model that has been used so far, such as a change in the classical tearing stability [6, 7, 26, 27], attempts to model the triggering of a NTM as a secondary mode remain unsuccessful [28]. Additional physics, coming for example from a two fluid description, could well be essential in the triggering process, allowing for example the polarization current to provide a destabilizing contribution. This could be the case if the seed mode has a frequency outside the range between electron and ion diamagnetic frequencies [29], as modelled in [30]. On the critical island width issue, the polarization effect is also expected to play a role, although in the absence of any external drive this effect should be stabilizing [19, 20, 31, 32], as suggested by experiment [3, 5]. Taking into account neoclassical ion viscosity leads to the enhancement of the polarization current effect [33], and this has also been shown to affect the NTM threshold in non linear MHD modelling [34].

In the present work, we restrict ourselves to the standard MHD model, thus ignoring diamagnetic and polarization effects. Despite the limitation of this MHD model, our comparison of full MHD non linear simulations of Neoclassical Tearing Modes with experimental observations on JET gives many encouraging results. In particular, we identify the increase of magnetic shear during current diffusion as a factor that facilitates NTM triggering, through the decrease of the critical width. Also, the dynamics of confinement degradation during the mode growth is consistent with the observation, and the mode identification from a synthetic diagnostic reveals similar features to experimental measurements. The NTMthreshold predicted by a Generalized Rutherford Equation is shown to be very sensitive to the model used for the tearing parameter Δ', and a reasonable agreement with quasi linear simulations can only be obtained if this parameter is small compared to curvature effect.

The paper is organized as follows: the physical model for non linear simulations as well as for the Rutherford model are presented in section 2, and the experiments that are analysed are described in section 3. The (2,1) NTM threshold determined from the models is discussed in section 4, and the non linear evolution is compared to experimental measurements in section 5.

2. PHYSICAL MODEL

The standard fluid MHD model equations with fixed density are solved in toroidal geometry:

$$\begin{aligned} \rho(\partial_t v + v\cdot\nabla v) &= J\times B - \nabla p + \nu\nabla^2 v \\ \partial_t p + v\cdot\nabla p + \Gamma p\nabla\cdot v &= \nabla\cdot\chi_\perp\nabla p + B\cdot\nabla[\chi_{/\!/}(B\cdot\nabla p)/B^2] + H \\ \partial_t B &= \nabla\times(V\times B) - \nabla\times\eta(J - J_{NI}) \end{aligned} \tag{1}$$

where $\mathbf{J_{NI}} = \mathbf{J_{cd}} + \mathbf{J_{bs}}$ is the non inductive current density, $\mathbf{J_{bs}}$ is the bootstrap current, $\mathbf{J_{cd}}$ is the imposed current source ($\mathbf{J_{cd}} = (\mathbf{J_{bs}} - \mathbf{J_{bs}})_{t=0}$), and $H = -\nabla\cdot\chi_\perp\nabla_p(t=0)$ is the heat source term. The bootstrap current is modelled as $\mathbf{J_{bs}} = f_x J_{bs}^{eq}(\nabla p(t)/\nabla p^{eq})\mathbf{B}/B$ with f_x a free parameter for rescaling the total bootstrap current J^{eq}_{bs}. Note that the equilibrium is not modified when varying f_x. The magnetic equilibrium itself is computed with the CHEASE code [35], which also provides the equilibrium bootstrap current. More details on the XTOR code can be found in [14].

The result is compared to the following form of the Rutherford equation, that covers the same physics as the code, i.e. includes curvature [18] and bootstrap [16] contributions:

$$0.82S^{-1}\frac{dW}{dt} = a\Delta'(w) - 6.35\frac{D_R}{\sqrt{W^2 + 0.65W_\chi^2}} + 6.35 f_x J_{bs}\frac{q}{s}\frac{W}{W^2 + (1.8W_\chi)^2} \tag{2}$$

where the various terms are evaluated at q = 2, S is the Lundquist number ($S = \tau_R/\tau_A$, with $\tau_R = \mu_0 a^2/\eta$ and $\tau_A = R_0\sqrt{\mu_0\rho}/B_0$), $J_{bs} \equiv (\mu_0 R_0/B_0)J_{bs}^{eq}$ with R_0 and B^0 the major radius and magnetic field at geometric axis, a the minor radius and $W \equiv w/a$. We also define $W_\chi = 2\sqrt{2}(\chi_\perp/\chi_{\|})^{1/4}/\sqrt{x\epsilon ns}$, with $x = \sqrt{\Phi}$ Φ, is the normalized toroidal flux, $s = d(\log q)/d(\log x)$ the magnetic shear and $\epsilon = a/R_0$. The resistive index DR is defined in [36], and its expression in the limit of small ϵ is [37]:

$$D_R = \frac{2\mu_0 q^2}{B^2 s^2}\left(-x\frac{dp}{dx}\right)\left[1 - \frac{1}{q^2} + \frac{q}{x^3}\frac{dq}{dx}\int_0^x d\bar{x}\left(\frac{\bar{x}^3}{q^2} - \frac{2\mu_0\bar{x}^2}{B^2\epsilon^2}\frac{dp}{d\bar{x}}\right)\right] \tag{3}$$

One important limitation coming from a Rutherford-type analysis is related to the choice of a model for the Δ' term. This parameter is defined in cylindrical geometry as

$$a\Delta'_{cyl.} = \lim_{\sigma\to 0}\frac{\psi'(x_s + \sigma) - \psi'(x_s - \sigma)}{\psi(x_s)}$$

with ψ the poloidal magnetic flux, and x_s the radial pos is obtained from the solution of the tearing equation

$$\frac{1}{x}\frac{d}{dx}\left(x\frac{d\psi}{dx}\right) - \left(\frac{m^2}{x^2} + \frac{\mu_0 q R_0 (dJ_z/dx)}{xB_0(1 - nq/m)}\right)\psi = 0 \tag{4}$$

with J_z the toroidal current density. Very often, Δ' is approximated by $a\Delta' = -2m/x$, which corresponds to the solution of the tearing equation without toroidal current density gradient ($dJ_z/dr = 0$). As we will see later (section 4.2), this simplification is generally not justified.

The physics of the classical tearing mode saturation, which can be represented in the form of a W-dependence of the tearing parameter Δ' (like $a\Delta'(W) = a\Delta'_0 - \alpha W$ [38, 39], or more complex closures [40]), is also ignored in the standard Generalized Rutherford Equation. For comparison with the approximation $a\Delta' = -2m/x$, we will also compute the solution of the Rutherford equation with the model derived in [40].

With our notations, the tearing parameter can then be expressed in this model as:

$$a\Delta'(W) = a\Delta'_{cyl.} + 0.82W\left\{\frac{A}{2}\left(A\log W + \frac{\Sigma}{2}\right) - 2.21A^2 + 0.4\frac{A}{x} + \frac{B}{2}\right\}$$

$$\begin{aligned} A &= \frac{dJ/dx}{J_z}\left(1 - \frac{2}{s}\right) \\ B &= \frac{d^2J/dx^2}{J_z}\left(1 - \frac{2}{s}\right) \\ \Sigma' &= \lim_{\sigma \to 0^+}\left(\frac{\psi'(x_s + \sigma) + \psi'(x_s - \sigma)}{\psi(x_s)} - 2A(1 + \log\sigma)\right) \end{aligned} \tag{5}$$

All terms are evaluated in the numerical resolution of the tearing equation 4, which uses finite elements and mesh accumulation at the resonance. A numerical difficulty comes with the Σ' term, which requires very dense mesh before converging. The convergence is established by increasing the number of finite element at a fixed σ value.

3. EXPERIMENTAL DATA

High-β_N discharges with q_{min} above unity have been extensively studied in JET, and have been often found to hit a soft (i.e. non disruptive) n = 1 MHD limit [41, 12, 13], that leads to confinement degradation of about 10-20% in the H factor .

For the present work, we have chosen two discharges operated at $q_{95} = 5$ but at different magnetic fields. The first discharge (Pulse No: 72668) is operated at B = 1.8T, I_p = 1.2MA. With 21MW of input power, the performance reaches $\beta_N \approx 2.8$. After a series of short bursts, attributed to q = 2 fishbones [12], the n = 1 mode develops and generates significant confinement degradation, with H89 lowered by about 15% (figure 1). The second discharge (Pulse No: 74226) is operated at B = 2.7T, I_p = 1.8MA and has also $q_{95} = 5$. The total input power is 23MW, and $\beta_N \approx 2.5$. Similar bursts of n = 1 mode are observed, but the soft MHD limitation is not triggered (figure 2).

In order to address the issue of resistive mode (meta)-stability in these discharges, we consider for the MHD limited case (PulseNo: 72668) the properties of the discharge one second before the mode triggering (at t = 6s), and at the mode triggering (at t = 7s).
The magnetic equilibrium is taken from EFIT reconstruction constrained by Motional Stark Effect (MSE), polarimetry and core pressure measurements. The advantage of this method is that it provides a smoothed solution of the Grad-Shafranov equation that fits (in the least mean square sense) the experimental measurements. Discharge simulation, as done by integrated codes like TRANSP [42] or CRONOS [43, 44], is another alternative that allows more detailed radial structures to be described, in a way that is consistent with particle, momentum, heat and current sources. But for the present study, where we want to highlight the essential feature of NTM properties, we have considered that details of the pressure profile could generate complicated (and maybe spurious) oscillations of the bootstrap contribution that would induce more confusion that clarification. Accordingly, we base our work on the EFIT reconstruction. However, we use other information from the discharge simulation done with TRANSP for Pulse No:72668. Heat diffusivity calculated from energy balance is an essential input for evaluating the relative dynamics of current and pressure, that can play a role in the NTM threshold (see section 4.1). The total bootstrap current calculated with the NCLASS module [45] is used for a more precise comparison with experiment in section 5.

For the study with XTOR, we have fitted the separatrix with an up/down symmetric shape (using a mean square root minimization). This has minor impact on the safety factor profile inside $\sqrt{\psi} = 0.95$, and we have imposed in CHEASE that the position of the q = 2 surface (in $\sqrt{\psi}$) is exactly that given by EFIT reconstruction. The safety factor profiles thus obtained are shown in figure 3. For the MHD-limited case (Pulse No: 72668), the evolution of the q-profile before the triggering of the n = 1 mode essentially reflects the diffusion of the current in the plasma, which is not steady-state. The central value of the safety factor evolves from q(0) = 1.55 to q(0) = 1.37, and the q = 2 surface moves from $\sqrt{\Phi} = 0.51$ to $\sqrt{\Phi} = 0.54$. The non MHD-limited case (Pulse No: 74226) has a q = 2 surface that is more inside the plasma, according to the reconstruction. Both cases have monotonic q-profiles, with q_{min} above unity, in agreement with the absence of sawtoothing activity.

4. (2,1) NTM THRESHOLD FROM MODELLING

We address in this section the issue of the non linear NTM threshold for the (2,1) mode, with comparison between the Rutherford prediction and quasi-linear (i.e. n = 0 and n = 1 only) MHD simulations using XTOR. Due to the importance of perpendicular diffusivity in the dynamics of pressure, we first investigate the role of this term in the determination of the critical island width.

4.1. ROLE OF PERPENDICULAR DIFFUSIVITY 4.1. ROLE OF PERPENDICULAR DIFFUSIVITY

The value of perpendicular diffusivity is mainly controlled, in tokamak plasmas, by the level of small scale and large spectrum turbulent transport. The dynamics of pressure evolves on a typical

time scale $\tau_E \propto a^2/\chi_\perp$, while the plasma current evolves on a time scalen $\tau_R = \mu_0 a^2/\eta$. In non linear MHD simulations, keeping the relative dynamics of pressure and current as they are in the experiment can be of importance [46]. But for NTM studies, this is mandatory, as pressure and current are coupled through the bootstrap current. This translates into conserving the product $S\chi_\perp$ as it is in the experiment (here as in the following, heat diffusivities are normalized to a^2/τ_A).

For a magnetic island, pressure effect is controlled by the ratio $\chi_\parallel/\chi_\perp$, which determines the critical width W_χ (already introduced) below which the effect of the island on the bootstrap current vanishes [16]. Another mechanism is however playing a role in the neoclassical island dynamics, as we will show here, and it concerns the effect of the island on the heat transport through the X-point.

In order to investigate the role of $\chi_\perp$ on the critical island, we take the equilibrium of Pulse No: 74226 at t = 7s, and run quasi-linear simulations with XTOR at $S(0) = 10^7$, $\nu = 10\eta(0)$ and a fixed ratio $\chi_\parallel/\chi_\perp = 10^8$. The bootstrap fraction in these simulations is $f_{bs} = 0.76$. The seed island is varied by steps of about $\Delta W \approx 0.004$ until the NTM branch is found (the step determines the corresponding error bar). The value of $\chi_\perp$ is scanned, and we find that in the low $\chi_\perp$ regime the critical island width decreases strongly (figure 4). The reason for this decrease is the reversal of the bootstrap current outside the island, which enhances the NTM drive. This is shown in figure 5, where a Poincaré section is plotted on the left, and the corresponding contour of the poloidal component of the bootstrap current is plotted on the right. The mechanism at play seems to be the following: heat transport is enhanced at the island X-point, and is rapidly equilibrated in the parallel direction outside the island. When perpendicular transport is small, the pressure inside the island is temporarily lower than outside, resulting in a reversal of the pressure gradient (and of the bootstrap current) at the island O-point. As a result, the island is destabilized below the level predicted when a flattening of the pressure is assumed. This effect is enhanced when the island grows faster. This has been checked by running simulations at different Lundquist numbers, as shown in figure 4.

As a result, although transport coefficients only appear through their relative amplitude in the Rutherford equation, the choice of $\chi_\perp$ can be of consequence for the determination of the critical island width. This is true in particular in the regime where perpendicular heat transport at the O-point is too small to compensate for the anomalous heat flux at the X-point.

Experimental values for $\chi_\perp$ are taken from a TRANSP simulation done for the case Pulse No: 72668. It gives $\chi_\perp \sim 1 m^2/s$ in the plasma centre, which in normalized units converts into $S\chi_\perp \approx 400$. Quasi linear XTOR calculations have been performed for the equilibrium Pulse No: 72668 at t = 7s with $f_{bs} = 0.76$, $S = 10^7$ and $\chi_\parallel/\chi_\perp = 10^8$. They show that W_{crit} remains similar ($W_{crit} \in [0.023, 0.029]$) when $\chi_\perp$ is varied in the range $\chi_\perp = [10^{-5}, 4 \times 10^{-5}]$. The (2,1) NTM is therefore in a regime where W_{crit} weakly depends on $\chi_\perp$, because the pressure flattening has enough time to take place during the mode growth. For the case Pulse No: 74226, we choose in the following $S\chi_\perp = 100$, for which Wcrit is also weakly dependent on $\chi_\perp$.

4.2. (2,1) NTM THRESHOLD: SIMULATION AND RUTHERFORD PREDICTION

4.2.1. Quasi linear results with XTOR

Numerical simulations are performed in a quasi-linear regime, i.e. retaining only n = 0 and n = 1, with a Lundquist number $S(0) = 10^7$ at the plasma centre. We deduce the perpendicular heat diffusivities from the relation $S\chi_\perp \approx (S\chi_\perp)^{exp.}$, and we take otherwise $\chi_\parallel/\chi_\perp = 10^8$ and a viscosity $\nu = 10\eta(0)$. The bootstrap fraction is varied using the rescaling parameter f_x applied to the bootstrap current computed with CHEASE, and the seed island is scanned until the NTM branch is found. The critical island width Wcrit for equilibria from Pulse No's: 74226 and 72668 is then determined as a function of the total bootstrap fraction fbs.

The result of the XTOR simulations is shown in figure 6. The critical island width for MHD stable cases (Pulse No's: 74226 and 72668 at t = 6s) is found to be similar, and of the order of $W_{crit} \sim 7.5\%$ at $f_{bs} \approx 0.4$. For the equilibrium where the (2,1) NTM is about to be triggered (Pulse No's: 72668 at t = 7s), the threshold is found to be significantly lower, with $W_{crit} \sim 5\%$ at $f_{bs} \approx 0.38$. From TRANSP/NCLASS, the bootstrap fraction is of this order, although slightly lower with $f_{bs} \approx 0.34$. Thus, we find that the triggering of a (2,1) NTM at t = 7s in the Pulse No: 72668 is consistent with modelling, assuming a constant (in time) level of seeding process, able to generate seed islands of about 5% of the minor radius.

4.2.2. The Rutherford-based evaluation: impact of the Δ′ model

These results have been compared with the solutions of the Rutherford equation, with different models for the Δ′ term. The simplest one assumes $a\Delta' = -m/x$, the second uses the solution of the tearing equation $a\Delta' = a\Delta'_{cyl.}$, and the third one takes the W-dependent model from [40] (see equation 5). The results are shown in figure 7 together with XTOR results for better comparison. The first thing to note is that all 2 models predict that the critical island width is lower at t = 7s compared to t = 6s for Pulse No: 72668, in agreement with XTOR result. The second point is that the Δ′ model does not play a significant role for Pulse No: 74226, and for this case the critical island width predicted by the Generalized Rutherford Equation is roughly in agreement with XTOR.

For the simplest evaluation of the Δ′ term ($a\Delta' = -m/x$), we find that the NTM branch appears only above $f_{bs} \sim 0.4$ for Pulse No: 72668. For $f_{bs} > 0.5$, the critical island width is in reasonable agreement with the XTOR simulations for the MHD stable cases. For the NTM triggered case (Pulse No: 72668 at t = 7s), the Rutherford evaluation predicts a lower threshold, but by far not as low as found with the XTOR simulations.

The cylindrical Δ′ is calculated by solving the Tearing equation in cylindrical geometry (equation 4), with an ideal wall at the plasma boundary (as in XTOR simulations). We compare in figure 8 the Δ′ value with and without the current density gradient for the case Pulse No: 72668, as a function of the radial position of the n = 1 and n = 2 resonant modes. The plot on the left shows that the useful simplification $a\Delta' = -m/x$ (corresponding to the gradient-free toroidal current solution of the Tearing equation) is largely underestimated. Indeed, the correct solution

of the tearing equation is large and positive, with $a\Delta'_{cyl.} \approx 38$ at t = 6s and $a\Delta'_{cyl.} \approx 28$ at t = 7s for the (2, 1) mode. The same remark applies for the n = 2 mode up to m = 4. As a consequence, the critical island width deduced from the Generalized Rutherford Equation is much smaller, and far below the XTOR results for the case Pulse No: 72668.

The W-dependent model for Δ' has finally been used. It naturally predicts critical island sizes above that obtained with $a\Delta'_{cyl}$. thanks to the W dependence, and therefore moves the prediction for Pulse No: 72668 closer to XTOR results. However, this correction appears to be too small in this particular case to allow recovering the results from quasi linear simulations. Note that the validity of this model requires $Wa\Delta' << 1$, and this condition is only marginally fulfilled for the Δ' equilibria from Pulse No: 72668, where $Wa\Delta' \leq 1$ implies $W \leq 0.026$ at t = 6s and $W \leq 0.036$ at t = 7s.

Finally, we have calculated the critical width by choosing a 2 = 0 in the Generalized Rutherford Equation. This crude model gives at the end a rather good agreement with non linear simulations for a total bootstrap fraction $f_{bs} \sim 0.4$, although we will not intend to generalize its applicability to more general context.

To conclude on this comparison between quasi-linear simulations and predictions based on a generalized Rutherford equation, it appears that significant discrepancies cannot be avoided, although the relative thresholds of the 3 equilibria that are analysed are correctly ordered: the critical island width of the unstable equilibrium is found to be lower than that of the two others. The reasons why the Generalized Rutherford Equation fails to predict the correct threshold are probably many, and could first be attributed to the absence of a self-consistent treatment of all physical effects. However, it is clear that an important factor of discrepancy comes from the Δ' term. Indeed, the Rutherford prediction is fairly good when the curvature term is large enough compared to Δ'. In order to illustrate this, we plot the (dW/dt,W) diagram from Rutherford equation in figure 9 for the 3 equilibria. The curvature term, which is proportional to D_R, will strongly depend on the local magnetic shear since $D_R \propto s^{-2}$ [37]. For the #74226 case, the magnetic shear at q = 2 is small ($s \approx 0.4$) and therefore the curvature term is large, with $D_R \approx 1.12$, so that at W = 0 the curvature term alone gives at the RHS of the Rutherford equation $RHS = 0.82S^{-1}dW/dt \approx -174$. This term is largely dominant over $a\Delta'$, which is $-2m/x_s \approx -11$ or $a\Delta'_{cyl.} \approx +10$ for the two extreme models. In contrast with this situation, the magnetic shear at q = 2 is much larger for the Pulse No: 72668, with $s \approx 0.78$ at t = 6s and $s \approx 1.04$ at t = 7s. The resistive index D_R is therefore smaller, with $D_R \approx 0.47$ at t = 6s and $D_R \approx 0.27$ at t = 7s, and the curvature term gives $RHS \approx -50$ at t = 6s and RHS ≈ “30 at t = 7s. In such condition, the contribution from 2 is no longer negligible and the result strongly depends on the model chosen for this term.

4.2.3. Role of current diffusion in the decrease of the critical island width

In order to better understand what causes the smaller critical island width as equilibrium evolves for Pulse No: 72668, we come back to the Rutherford analysis, using the evaluation $a\Delta' = 0$, i.e. ruling out the Δ' contribution to the problem. With this limitation, we find that the reduction of the

critical width for NTM triggering originates from an increasing magnetic shear s at q = 2, as the current diffuses into the plasma. This increase of $s_{q=2}$ decreases $W\chi$ as well as the curvature stabilisation term D_R, as can be modelled using the main dependencies in x and s: $D_R \propto xp'/s^2$, $W\chi \propto 1/\sqrt{xs}$, $J_{bs} \propto -\sqrt{x}p'/x$, and assuming a pressure profile $p = p_0(1-x^2)2$. The critical island width is then evaluated from the static unstable solution of the Rutherford equation around the equilibrium data from Pulse No: 72668 at t = 7s. Between t = 6s and t = 7s, the q = 2 surfaces moves outwards (stabilizing) but the dominant effect is the increase of the magnetic shear (destabilizing), as shown in the figure 10.

4.2.4. Summary

In summary, we find that triggering of a (2,1) NTM in Pulse No: 72668 is consistent with a seeding process producing seed island of about 5% of the minor radius at q = 2, with a critical island width decaying with time as current diffuses in the discharge. This decay is partly explained by the destabilizing effect of increasing magnetic shear, which lowers the curvature term $D_R \propto 1/s^2$, although unfavourable evolution of the tearing stability (represented by the Δ' term in Rutherford equation) probably contributes to the lowering of W_{crit}, as can be inferred from the lower Wcrit from XTOR compared to the Rutherford prediction. The comparison with a different equilibrium (Pulse No: 74226) where q = 2 is more inside (unfavourable) but with lower magnetic shear (favourable) shows that the Rutherford evaluation is improved when curvature effects are dominant, i.e. when the magnetic shear is low at the resonance.

5. NON-LINEAR SIMULATIONS AND COMPARISON TO EXPERIMENT

Non linear simulations have been performed for the equilibrium of Pulse No: 72668 at t = 7s, with a total bootstrap fraction $f_{bs} = 0.38$, similar to the one calculated in TRANSP. With this case, the dynamics of the confinement degradation and the radial structure of the temperature perturbation can be compared with experimental observations. The computed spectrum covers toroidal mode numbers n = 0 ... 6 and poloidal mode numbers m = 0... 64. Later in the non linear regime, we had to extend the description to n = 0...12 and m = 0...96. Note that the island width cannot be evaluated rigorously at every time step, because an ergodic region appear around the separatrix in the non linear regime, preventing the determination of the separatrix from a Poincaré plot. We therefore calculate the island width after evaluating the constant C in the relation $W_{(2,1)} = C E_{(2,1)}^{1/4}$ (with $E_{(2,1)}$ the magnetic energy of the (2, 1) mode) in the linear regime.

We have first checked if the critical island width was similar in the non linear and quasi linear runs. As shown in figure 11, Wcrit tends to be slightly lower in the non linear simulation (W_{crit} = 0.0467±0.0012) than in the quasi-linear ones (W_{crit} = 0.0499±0.0011). Non linear coupling tends therefore to facilitate the triggering of the NTM, because harmonics of the dominant mode help in flattening the pressure at the O-point. The comparison of the lowest non linearly unstable seed (▲) with the quasi linear run shows that it takes about $5\times10^3\tau_A$ for this process to drive the mode unstable

when it was found stable in the quasi linear regime. We also compare simulations with a seed in the unstable domain (▲). Here, we find that non linear coupling slows the growth of the q = 2 island.

5.1. CONFINEMENT DEGRADATION DUE TO THE (2,1) NTM

In the experiment, the confinement degradation takes place in about 1 second, and is in the range 40-50% for ion and electron pressures (figure 1). We compare the dynamics of the confinement degradation and its amplitude with our non linear simulation. In the non linear regime, the (2, 1) NTM is found to generate a large stochastic region, resulting in a significant confinement degradation. For a bootstrap fraction $f_{bs} = 0.38$ (comparable with the TRANSP calculated value), the core pressure is reduced by about 15% at the latest simulation step (figure 12). The Poincaré map shows that flux surfaces are largely ergodized around q = 2, leaving only two holes for identifying the poloidal mode number. Among other island chains, a (3, 2) island is also clearly identified. The saturation is not yet reached at the latest simulation steps, and we did not pursue it because of limited computing time. However, the time constant of the confinement degradation is similar in the experiment and in the simulation. This can be verified by rescaling the simulation dynamics according to $\Delta t = (S^{exp.}/S^{sim.})\ \tau_A \Delta t$. According to this renormalisation, $10^4 \tau_A$ in the simulation corresponds to ~ 300ms. More precisely, we have applied the transformation:

$$t^{exp} = 3.4 \times 10^4\ (t^{exp} - t^0)$$

with $t^0 = 7.06$s the time when the (2, 1) mode is triggered. With this rescaling, we can compare the experimental evolution of the pressure measured from various means with what is found in the simulation. In figure 12, we plot the evolution of electron pressure measured by the LIDAR diagnostic (LIDR), the ion pressure measured by Charge Exchange diagnostic (CX), and the total pressure determined by the EFIT reconstruction. All pressures are normalized to their value at the time of the mode triggering for clarity. As can be seen, the dynamics of pressure is relatively well reproduced by the simulation. Note that increasing the bootstrap fraction accelerates the pressure drop (grey dashed line in figure 12).

5.2. Electron temperature fluctuations

The mode structure is well diagnosed by electron temperature fluctuations in the experiment. The Electron Cyclotron Emission (ECE) radiometer in JET provides a measurement of electron temperature along an horizontal line of sight at the tokamak geometrical midplane, which does not coincide with the magnetic axis position [47]. In the following, the mode structure is determined from a wavelet analysis of the ECE signal. The amplitude A and phase Θ of the perturbation is calculated for each ECE channel along the evolving frequency of the dominant mode f(t), and the mode structure is calculated as $\delta T_e(R, t) = A(f(t)) \times \cos(\ (f(t)) - \Theta_0(f(t)))$, where $\Theta_0(f(t))$ is the phase at a reference position where the mode amplitude is large.

Analysis of the MHD mode structures at different times after its triggering at t = 7.06s is shown

in figure 13. We shall first remark that a small n = 2 mode is already present in the plasma when the (2, 1) mode is triggered. We find that the n = 1 mode is initially strongly coupled to this pre-existing n = 2 mode (presumably localized on q = 5/2), and then it grows uncoupled. The relative amplitude $\delta T_e/T_e(0)$ is from the early stage of the mode evolution around 2%. The interpretation of these structures is not simple due to the off-axis line of sight of the diagnostic, and the comparison with a synthetic diagnostic implemented in the non linear simulations is useful.

5.3. Radial structure of the (2,1) NTM in the simulation

We have implemented a simplified synthetic diagnostic for pressure fluctuations in XTOR output, where the effect of an off-axis line of sight can be studied. The temperature fluctuation produced by the rotation of the MHD mode passing in front of the diagnostic is analogous to exploring the pressure along the toroidal angle: $\delta T_e(R, t) \Leftrightarrow p(R, \varphi)$. The analysis program is the same as the one used for obtaining the temperature fluctuation from ECE in figure 13, and the reference phase is taken here at R/a = 4 where the fluctuation amplitude is maximum. In normalised units, the line of sight of the ECE radiometer is at Z/a = –0.22. Note that the pressure perturbation is equivalent to the temperature perturbation since the density is constant in the simulation.

In order to show the impact of the off-axis line of sight on the mode structure determination, we compare the pressure perturbation calculated along a line of sight crossing the magnetic axis at $Z = Z_{mag}$, with the same quantity calculated along the equivalent ECE radiometer line of sight. The radial profiles determined under the two diagnostic configurations are shown in figure 14, for the non linear simulation at $t = 17641\tau_A$. The even parity of the n = 1 mode structure is clearly identified when the line of sight crosses the magnetic axis, and converts to an apparent odd parity for the off-axis line of sight, similar to experimental findings shown in figure 13.

The mode structure is shown at various times in figure 15. The relative amplitude of the perturbation is, from the early stage of the mode growth, of the order of 2%. It does increase slightly as the island grows, more than measured in the experiment, and it does not change much in shape. From the ECE diagnostic, it is not easy to determine the probable q = 2 surface position before t = 7.28s, where the inversion radius seems to be around R = 3.35m (along the diagnostic line of sight). In contrast, we have the q = 2 island more outward, around R = 3.5m. The radial profile of the mode compares well with the experiment inside the resonance, but the structure outside the resonance evolves differently. In the experiment, no clear inversion can be seen during the first 0.25s, and it develops afterwards in a broad region R = 3.35≈3.5m. In the simulation, the inversion radius is never clearly identified at q = 2 on the Low Field Side (LFS at R ≈ 3.5m), while this signature of the island position appears clearly on the High Field Side (HFS at R ≈ 2.5m).

To summarize, the comparison of mode structures shows similarities but also important differences. The relative amplitude of the n = 1 perturbation is well reproduced, and its radial profile inside q = 2 is similar to the observed one. Interestingly, the differences give some clues on physical phenomenon that are not covered in the present MHD modelling and may play an important role in the dynamics of the NTM.

The first discrepancy concerns the position of resonant modes, and it is not related to the MHD model. Inaccuracy of the input equilibrium is of course a main source of error for all MHD studies, and this could well produce this mismatch. However, we also need to consider error bars in the position of the ECE channels when appreciating this difference. This error is typically of the order of 2–5cm for typical JET plasmas [47] but could be more important in certain cases as suggested by a statistical analysis [48]. Adding these two uncertainties may explain the large difference (about 15cm) in the q = 2 position, although it may be difficult to determine which is the dominant source of error.

The second difference concerns the n = 1 mode structure outside the q = 2 resonance, which as mentioned previously does not show a clear sign of an inversion radius on the outboard side. This difference with experimental observations is due to the q = 3 island, as evidenced by the odd parity of the distorsion outside q = 2 (see figure 14, with the on-axis line of sight of the plot on the left): it reinforces the inversion at q = 2 on the High Field Side and weakens it on the Low Field Side. A possible explanation for the absence of such signature of an island on q = 3 is that toroidal coupling between the two poloidal harmonics is prevented by the differential rotation between the two resonances, so that the MHD displacement at q = 3 is much weaker than in the simulation. This issue is outside the scope of the present paper, as toroidal rotation is ignored. However, with a central rotation of about 280km/s which represents about 7% of the Alfvén speed (see figure 16), this is certainly an effect that is worth considering in the future.

The third difference concerns the n = 2 mode. The fact that we do not recover the (5, 2) mode is not surprising, since the n = 2 mode is linearly stable in the input equilibrium, as we have checked with quasi linear runs (using n = 0 and n = 2 only). We did not expect, therefore, to find an island at q = 5/2 in the simulation. The growth of the (3, 2) mode, attested by the Poincar´e map (figure 12) as well as by the n = 2 mode structure (figure 14), is a more significant discrepancy. The linear stability of the n = 2 mode implies that the (3, 2) mode has a NTM nature, and that it is non linearly destabilized by the (2, 1) NTM. Although not consistent with the experiment it is supposed to reproduce, this is a demonstration of NTM triggering by non linear coupling in numerical simulation. For the (3, 2) NTM growth, the driving mode is the large (4, 2) component, which does not seem to be as large in the experiment. It is present in the early stage of the mode growth (figure 13, first plot), where it has the same amplitude as the (2, 1) mode, but it vanishes at later times, except a very minor contribution (compared to the outer component on q = 5/2) when the n = 1 mode is well developed (figure 13, last plot). There is a possibility that toroidal rotation shear plays a role here again. The pre-existing n = 2 mode, which is driven by the (5, 2) mode, may prevent the growth of a (4, 2) component that would rotate at a different velocity. The absence of a (3, 2) island would follow. Note that uncertainties in the input equilibrium, which may be wrong in predicting the presence of a q = 3/2 surface, would not solve the discrepancy on the (4, 2) component.

CONCLUSION AND PERSPECTIVES

The (2,1) NTM threshold in high performance JET discharges with q > 1 has been modelled with a non linear MHD code and compared to the prediction given by a Generalized Rutherford Equation.

We find that the determination of the critical island width can be sensitive to the perpendicular diffusivity taken in the simulation if it is too small, but with the rescaling $(\tau_R/\tau_A)^{sim.} = (\tau_R/\tau_A)^{exp.}$ that is mandatory for NTM modelling, the critical island width is relatively insensitive to the actual value of $\chi_\perp$, at fixed ratio $\chi_\parallel/\chi_\perp$. For the experiment that is studied, we find that the triggering of the (2,1) mode is consistent with the excitation of the NTM branch by a seed of about 5% of the minor radius. By comparing the threshold at the mode triggering time and one second before, we find that the diffusion of the plasma current plays a role in the lowering of the threshold, by reducing the curvature stabilisation effect through the increase of the local magnetic shear. The comparison with the prediction from a Generalized Rutherford Equation covering the same physical ingredients shows that when curvature effects are not sufficiently large, the result becomes very sensitive to the model used for the Δ' term, and is generally not very accurate. Finally, the non linear evolution of the (2,1) NTM has been compared with experimental observations. The dynamics of the confinement degradation is found to be qualitatively correct, with a long characteristic time. A synthetic ECE diagnostic implemented in the code shows the impact of the off-axis line of sight of the JET ECE radiometer on the identification of the mode. For the (2,1) NTM, we find comparable mode structure with a relative perturbation $\delta T/T \sim 2\%$, although the radial localisation of the q = 2 surface taken from the equilibrium code EFIT may be at a too large radius. The n = 2 mode that is observed outside q = 2 in the experiment (presumably at q = 5/2), develops at q = 3/2 in the simulation, and is excited non linearly by the (2,1) NTM. This discrepancy could result also from the sensitivity to the input equilibrium, which in the experiment may not contain the q = 3/2 surface. For both n = 1 and n = 2 modes, discrepancies on the radial profile of the mode structure suggest a stabilizing role of the toroidal rotation shear, which can decouple poloidal harmonics.

Several potentially important effects have been neglected for simplicity and need to be addressed in the future. As we just mentioned, the toroidal rotation in these plasmas is significant (about 7% of the Alfvén speed), and although it is very similar in the two discharges that have been considered here, it could affect the absolute value of the seed required to excite the (2,1) NTM, its non linear evolution and its impact on the confinement. The other aspect is the completeness of the MHD model. Separate density and temperature evolutions, rotation and two fluid effects, can be addressed in simulations based on a fully implicit numerical scheme, as developed in a recent version of XTOR [49], and should allow better comparison with experimental observations.

ACKNOWLEDGMENTS

Part of the XTOR runs has been performed on NEC-SX6 at the Centre de Calcul Recherche et Technologie, held by CEA. This work was carried out within the framework the European Fusion Development Agreement (EFDA) and the French Research Federation for Fusion Studies (FR-FCM). It is supported by the European Communities under the contract of Association between Euratom and CEA. The views and opinions expressed herein do not necessarily reflect those of the European Commission.

REFERENCES

[1]. Z. Chang, J.D. Callen, E.D. Fredrickson, R.V. Budny, C.C. Hegna, K.M. McGuire, M.C. Zarnstorff, and TFTR group. Observation of nonlinear neoclassical pressure-gradient driven tearing modes in TFTR. Physics Review Letters **74**(23):4663–4666, Jun 1995.

[2]. JET Team (prepared by G.T.A. Huysmans). Observation of neoclassical tearing modes in JET. Nuclear Fusion, **39**(11Y):1965–1970, 1999.

[3]. R.J. La Haye and O. Sauter. Threshold for metastable tearing modes in DIII-D. Nuclear Fusion, **38**(7):987–999, 1998.

[4]. A. Isayama, Y. Kamada, S. Ide, K Hamamatsu, T. Oikawa, T. Suzuki, Y. Neyatani, T. Ozeki, Y. Ikeda, K. Kajiwara, and the JT-60 team. Complete stabilization of a tearing mode in steady state high-βp H-mode discharges by the first harmonic electron cyclotron heating/current drive on JT-60U. Plasma Physics and Controlled Fusion, **42**(12):L37–L45, 2000.

[5]. R.J. Buttery, M. Valovic, C.D. Warrick, H.R. Wilson, COMPASS-D Team, and ECRH Teams. Controlled seeding of neoclassical tearing modes in COMPASS-D. Nuclear Fusion, **41**(8):985–994, 2001.

[6]. D.A. Kislov, Yu.V. Esipchuk, N.A. Kirneva, I.V. Klimanov, Yu.D. Pavlov, A.A. Subbotin, V.V. Alikaev, A.A. Borshegovskiy, Yu.V. Gott, A.M. Kakurin, S.V. Krilov, T.B. Myalton, I.N. Roy, E.V. Trukhina, V.V. Volkov, and T-10 Team. Beta limit due to resistive tearing modes in T-10. Nuclear Fusion, **41**(11):1619–1624, 2001.

[7]. H. Reimerdes, O. Sauter, T. Goodman, and A. Pochelon. From current-driven to neoclassically driven tearing modes. Physics Review Letters, **88**(10):105005, Feb 2002.

[8]. H.R. Koslowski, G. Fuchs, R. Jaspers, A. Kr¨amer-Flecken, A.M. Messiaen, J. Ongena, J. Rapp, F.C. Sch¨uller, and M.Z. Tokar. MHD activity at the beta limit in RI mode discharges on TEXTOR-94. Nuclear Fusion, **40**(4):821, 2000.

[9]. R. Carrera, R. D. Hazeltine, and M. Kotschenreuther. Island bootstrap current modification of the nonlinear dynamics of the tearing mode. Physics of Fluids, **29**(4):899–902, 1986.

[10]. T.C. Hender, J.C Wesley, J. Bialek, A. Bondeson, A.H. Boozer, R.J. Buttery, A. Garofalo, T.P Goodman, R.S. Granetz, Y. Gribov, O. Gruber, M. Gryaznevich, G. Giruzzi, S. G¨unter, N. Hayashi, P. Helander, C.C. Hegna, D.F. Howell, D.A. Humphreys, G.T.A. Huysmans, A.W. Hyatt, A. Isayama, S.C. Jardin, Y. Kawano, A. Kellman, C. Kessel, H.R. Koslowski, R.J. La Haye, E. Lazzaro, Y.Q. Liu, V. Lukash, J. Manickam, S. Medvedev, V. Mertens, S.V. Mirnov, Y. Nakamura, G. Navratil, M. Okabayashi, T. Ozeki, R. Paccagnella, G. Pautasso, F. Porcelli, V.D. Pustovitov, V. Riccardo, M. Sato, O. Sauter, M.J. Schaffer, M. Shimada, P. Sonato, E.J. Strait, M. Sugihara, M. Takechi, A.D. Turnbull, E. Westerhof, D.G. Whyte, R. Yoshino, H. Zohm, the ITPA MHD, Disruption, and Magnetic Control Topical Group. Chapter 3: MHD stability, operational limits and disruptions. Nuclear Fusion, **47**(6):S128–S202, 2007.

[11]. T.S. Taylor. Physics of advanced tokamaks. Plasma Physics Controlled Fusion, **39**:B47, 1997.

[12]. P. Buratti, R.J.Buttery, C.D.Challis, F.Crisanti, M.Gryaznevich, T.C.Hender, D.F.Howell,

E.Joffrin, J.Hobirk, F.Imbeaux, X.Litaudon, J.Mailloux, and JET-EFDA contributors. MHD stability limit analysis in JET high- n advanced scenarios. Sofia (Bulgaria), 2009. 36th EPS Conf. on Plasma Physics, Sofia (Bulgaria), (O2.007), European Physical Society.

[13]. C.D. Challis, B. Alper, M. Baruzzo, J. Bucalossi, P. Buratti, R. Buttery, M. Brix, G. Calabro, R. Cesario, F. Crisanti, J. Ferron, O. Ford, C. Giroud, M. Gryaznevich, T.C. Hender, J. Hobirk, D. Howell, F. Imbeaux, I. Jenkins, E. Joffrin, H. Leggate, T. Luce, D. McDonald, M. Murakami, V. Pericoli-Ridolfini, M. Tsalas, P de Vries, and JET EFDA contributors. Stability and confinement optimisation in the range q_0 = 1-3 at JET. Sofia (Bulgaria), 2009. 36th EPS Conf. on Plasma Physics, Sofia (Bulgaria), (P5.172), European Physical Society.

[14]. Hinrich Lütjens and Jean-Fran¸cois Luciani. The XTOR code for nonlinear 3D simulations of MHD instabilities in tokamak plasmas. J. Comp. Phys., **227**(14):6944–6966, 2008.

[15]. P. H. Rutherford. Nonlinear growth of the tearing mode.–Physics of Fluids, **16**(11):1903–1908, 1973.

[16]. Richard Fitzpatrick. Helical temperature perturbations associated with tearing modes in tokamak plasmas. Physics of Plasmas, **2**(3):825–838, 1995.

[17]. M. Kotschenreuther, R.D. Hazeltine, and P.J. Morrison. Nonlinear dynamics of magnetic islands with curvature and pressure.–Physics of Fluids, **28**(1):294–302, 1985.

[18]. Hinrich Lütjens, Jean-François Luciani, and Xavier Garbet. Curvature effects on the dynamics of tearing modes in tokamaks. Physics of Plasmas, **8**(10):4267–4270, 2001.

[19]. A. I. Smolyakov, A. Hirose, E. Lazzaro, G. B. Re, and J. D. Callen. Rotating nonlinear magnetic islands in a tokamak plasma. Physics of Plasmas, **2**(5):1581–1598, 1995.

[20]. H.R. Wilson, M. Alexander, J.W. Connor, A.M. Edwards, D. Gates, O. Grüber, R.J. Hastie, C.C. Hegna, T.C. Hender, R.J. La Haye, L.L. Lao, A.W. Morris, C.M. Roach, E.J. Strait, T.S. Taylor, M. Valovic, and H. Zohm. The collisionality dependence of tokamak -limits. Plasma Physics and Controlled Fusion, **38**(12A):A149–A163, 1996.

[21]. O. Sauter, R.J. La Haye, Z. Chang, D.A. Gates, Y. Kamada, H. Zohm, A. Bondeson, D. Boucher, J.D. Callen, M.S. Chu, T.A. Gianakon, O. Gruber, R.W. Harvey, C.C. Hegna, L.L. Lao, D.A. Monticello, F. Perkins, A. Pletzer, A.H. Reiman, M. Rosenbluth, E.J. Strait, T.S. Taylor, A.D. Turnbull, F. Waelbroeck, J.C. Wesley, H.R. Wilson, and R. Yoshino. Beta limits in long-pulse tokamak discharges. volume 4, pages **1654–1664**. AIP, 1997.

[22]. F. Militello, M. Ottaviani, and F. Porcelli. Neoclassical tearing mode saturation in periodic current sheets. Physics of Plasmas, **15**(4):042104, 2008.

[23]. Hinrich Lütjens, Jean-Fran¸cois Luciani, and Xavier Garbet. Nonlinear three-dimensional MHD simulations of tearing modes in tokamak plasmas. Plasma Physics and Controlled Fusion, **43**(12A):A339–A348, 2001.

[24]. Hinrich Lütjens and Jean-François Luciani. Saturation levels of neoclassical tearing modes in International Thermonuclear Experimental Reactor plasmas. Physics of Plasmas, **12**(8):080703, 2005.

[25]. Hinrich Lütjens and Jean-François Luciani. Stochastic couplings of neoclassical tearing modes in ITER plasmas. Physics of Plasmas, **13**(11):112501, 2006.

[26]. Patrick Maget, Jean-François Artaud, Lars-Goran Eriksson, Guido Huysmans, A. Lazaros, Philippe Moreau, Maurizio Ottaviani, Jean-Luc S´egui, andWolfgang Zwingmann. MHD activity triggered by monster sawtooth crashes on Tore Supra. Plasma Phys. Control. Fusion , 47:357–377, 2005.

[27]. D.P. Brennan, R.J. La Haye, A.D. Turnbull, M.S. Chu, T. H. Jensen, L.L. Lao, T.C. Luce, P. A. Politzer, E.J. Strait, S.E. Kruger, and D.D. Schnack. A mechanism for tearing onset near ideal stability boundaries.–Physics of Plasmas, **10**(5):1643–1652, 2003.

[28]. D.P. Brennan, S.E. Kruger, T.A. Gianakon, and D.D. Schnack. A categorization of tearing mode onset in tokamaks via nonlinear simulation. Nuclear Fusion, 45(9):1178–1190, 2005.

[29]. J.W. Connor, F.L. Waelbroeck, and H.R. Wilson. The role of polarization current in magnetic island evolution. Physics of Plasmas, **8**(6):2835–2848, 2001.

[30]. N. Arcis and S.E. Sharapov. Mechanism of neoclassical tearing modes triggering by a magnetic perturbation. Physics Letters A, **372**(36):5807–5810, 2008.

[31]. R. Fitzpatrick, F. L. Waelbroeck, and F. Militello. The influence of the ion polarization current on magnetic island stability in a tokamak plasma.–Physics of Plasmas, **13**(12):122507, 2006.

[32]. E. Lazzaro. Symmetry breaking and self-consistent rotation of magnetic islands in neoclassical viscous regimes. Physics of Plasmas, **16**(9):092504, 2009.

[33]. A.I. Smolyakov and E. Lazzaro. On neoclassical effects in the theory of magnetic islands. Physics of Plasmas, **11**(9):4353–4360, 2004.

[34]. T.A. Gianakon, S.E. Kruger, and C.C. Hegna. Heuristic closures for numerical simulations of neoclassical tearing modes. Physics of Plasmas, **9**(2):536–547, 2002.

[35]. H. Lütjens, A. Bondeson, and O. Sauter. The CHEASE code for toroidal MHD equilibria. Computer Physics Communications, **97**(3):219–260, 1996.

[36]. A.H. Glasser, J.M. Greene, and J.L. Johnson. Resistive instabilities in general toroidal plasma configurations. Physics of Fluids, **18**(7):875–888, 1975.

[37]. A.H. Glasser, J.M. Greene, and J.L. Johnson. Resistive instabilities in a tokamak. Physics of Fluids, **19**(4):567–574, 1976.

[38]. D. F. Escande and M. Ottaviani. Simple and rigorous solution for the nonlinear tearing mode. Physics Letters A, **323**(3-4):278 – 284, 2004.

[39]. F. Militello and F. Porcelli. Simple analysis of the nonlinear saturation of the tearing mode. Physics of Plasmas, **11**(5):L13–L16, 2004.

[40]. N. Arcis, D. F. Escande, and M. Ottaviani. Rigorous approach to the nonlinear saturation of the tearing mode in cylindrical and slab geometry. Physics of Plasmas, **13**(5):052305, 2006.

[41]. J. Mailloux, X. Litaudon, P. de Vries, B. Alper, Yu. Baranov, M. Baruzzo, M. Brix, P. Buratti, G. Calabro, R. Cesario, C.D. Challis, K. Crombe, O. Ford, D. Frigione, J. Garcia, C. Giroud, D. Howell, Ph. Jacquet, I. Jenkins, E. Joffrin, K. Kirov, P. Maget, D. C. McDonald, V. Pericoli-

Ridolfini, V. Plyusnin, F. Rimini, F. Sartori, M. Schneider, S. Sharapov, C. Sozzi, I. Voitsekovitch, L. Zabeo, M. K. Zedda, and JET-EFDA contributors. Development of a steady-state scenario in JET with dimensionless parameters approaching ITER target values. Sofia (Bulgaria), 2009. 36th EPS Conf. on Plasma Physics, Sofia (Bulgaria), (P5.164), European Physical Society.

[42]. R.J. Goldston, D.C. McCunea, H.H. Towner, S.L Davis, R.J. Hawryluk, and G.L. Schmidt. New techniques for calculating heat and particle source rates due to neutral beam injection in axisymmetric tokamaks. J. Comput. Phys., **43**:61, 1981.

[43]. V. Basiuk, J.F. Artaud, F. Imbeaux, X. Litaudon, A. Bécoulet, L.-G. Eriksson, G.T. Hoang, G. Huysmans, D. Mazon, D. Moreau, and Y. Peysson. Simulations of steady-state scenarios for Tore Supra using the CRONOS code. Nuclear Fusion, **43**(9):822–830, 2003.

[44]. J.F. Artaud, V. Basiuk, F. Imbeaux, M. Schneider, J. Garcia, G. Giruzzi, P. Huynh, T. Aniel, F. Albajar, J.M. Ané, A. Bécoulet, C. Bourdelle, A. Casati, L. Colas, J. Decker, L.G. Eriksson, X. Garbet, R. Guirlet, P. Hertout, G.T. Hoang,W. Houlberg, G. Huysmans, E. Joffrin, S.H. Kim, F. K¨ochl, J. Lister, X. Litaudon, P. Maget, R. Masset, B. Pégourié, Y. Peysson, P. Thomas, E. Tsitrone, and F. Turco. The CRONOS suite of codes for integrated tokamak modelling. submitted to Nuclear Fusion, 2009.

[45]. W.A. Houlberg, K.C. Shaing, S. P. Hirshman, and M.C. Zarnstorff. Bootstrap current and neoclassical transport in tokamaks of arbitrary collisionality and aspect ratio. Physics of Plasmas, **4**(9):3230–3242, 1997.

[46]. P. Maget, G.T.A. Huysmans, X. Garbet, M. Ottaviani, H. Lütjens, and J.-F. Luciani. Nonlinear Magnetohydrodynamic simulation of Tore Supra hollow current profile discharges.–Physics of Plasmas, **14**(5):052509, 2007.

[47]. E. de la Luna, J. Sánchez, V. Tribaldos, JET-EFDA contributors, G. Conway, W. Suttrop, J. Fessey, R. Prentice, C. Gowers, and J. M. Chareau. Electron cyclotron emission radiometer upgrade on the Joint European Torus (JET) tokamak. Review of Scientific Instruments, **75**(10):3831–3833, 2004.

[48]. B. Alper, L. Barrera, M. Baruzzo, A. Botrugno, P. Buratti, L. Figini, D.F. Howell, C. Giroud, E. De La Luna, O. Tudisco, and JET-EFDA contributors. MHD mode localisation in the JET tokamak. Sofia (Bulgaria), 2009. 36th EPS Conf. on Plasma Physics, Sofia (Bulgaria), (P5.169), European Physical Society.

[49]. Hinrich Lütjens and Jean-François Luciani. XTOR-2F: A fully implicit Newton-Krylov solver applied to nonlinear 3D bifluid MHD in tokamaks. submitted to J. Comp. Phys., 2009.

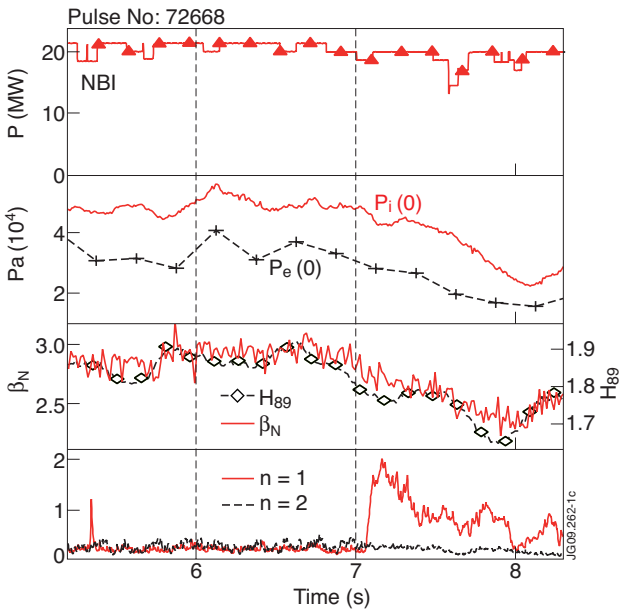

Figure 1: High-β_N JET discharge limited by n = 1 mode ($B = 1.8T$, $I_p = 1.2MA$, $q_{95} = 5$, $P_{tot} = 21MW$).

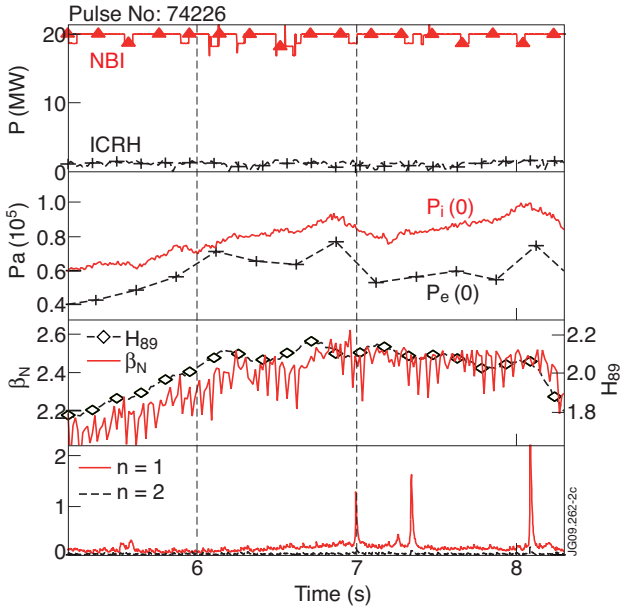

Figure 2: High- N JET discharge without n = 1 MHD limitation ($B = 2.7T$, $I_p = 1.8MA$, $q_{95} = 5$, $P_{tot} = 23MW$).

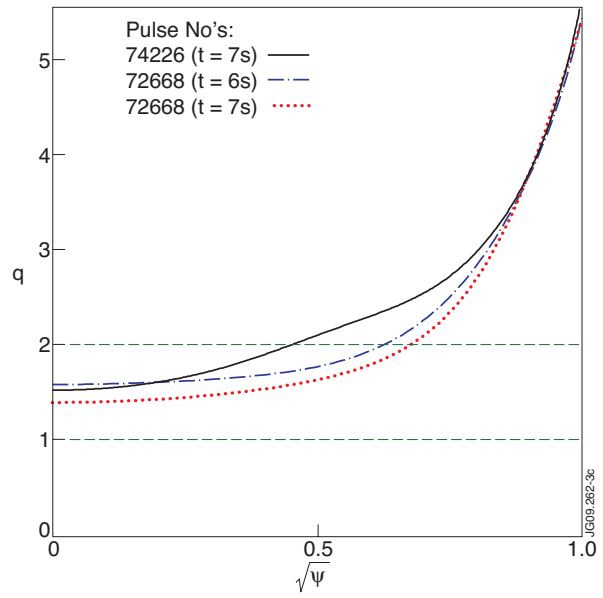

Figure 3: Safety factor profiles used in the study.

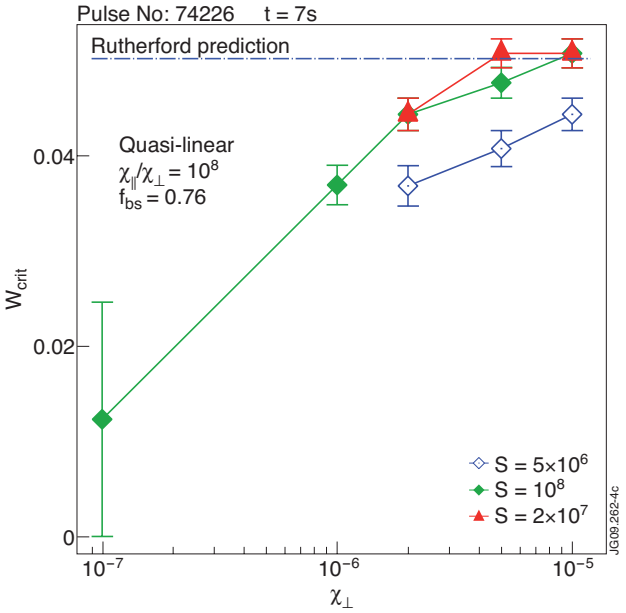

Figure 4: Critical island width as a function of $\chi_\perp$, while keeping $\chi_\parallel/\chi_\perp$ constant ($a\Delta' = -2m/x$ is assumed for the Rutherford prediction). The error bars correspond to the step in W.

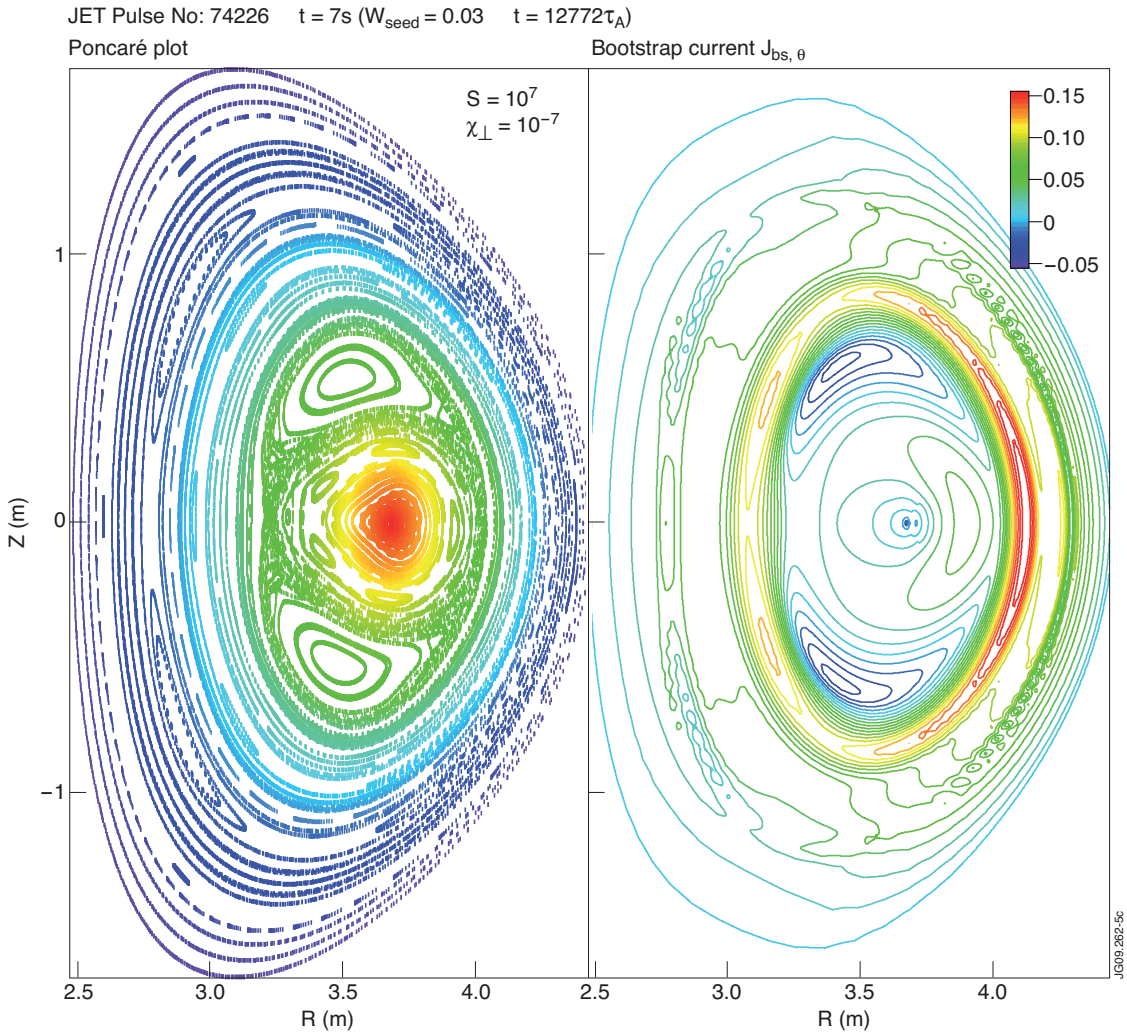

Figure 5: Poincaré section (left) and contours of the poloidal component of the bootstrap current (right) in a low $\chi_\perp$ regime where the critical island width is sensitive to the value of $\chi_\perp$ (at fixed $\chi_\parallel/\chi_\perp$).

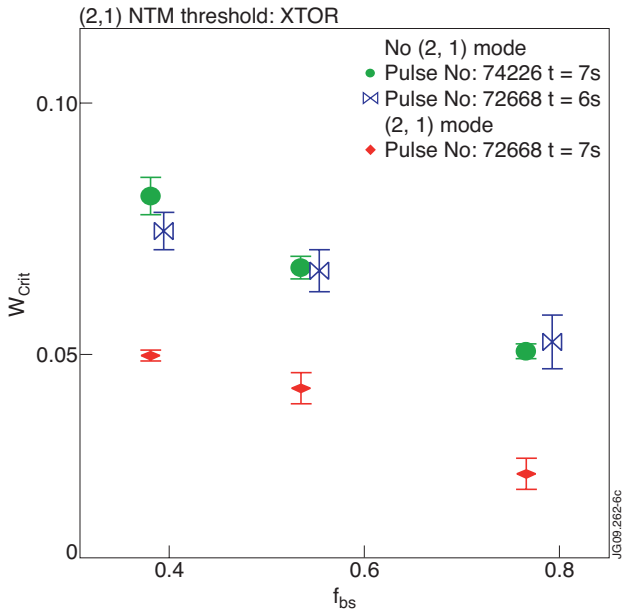

Figure 6: Critical island width as a function of the bootstrap fraction from XTOR.

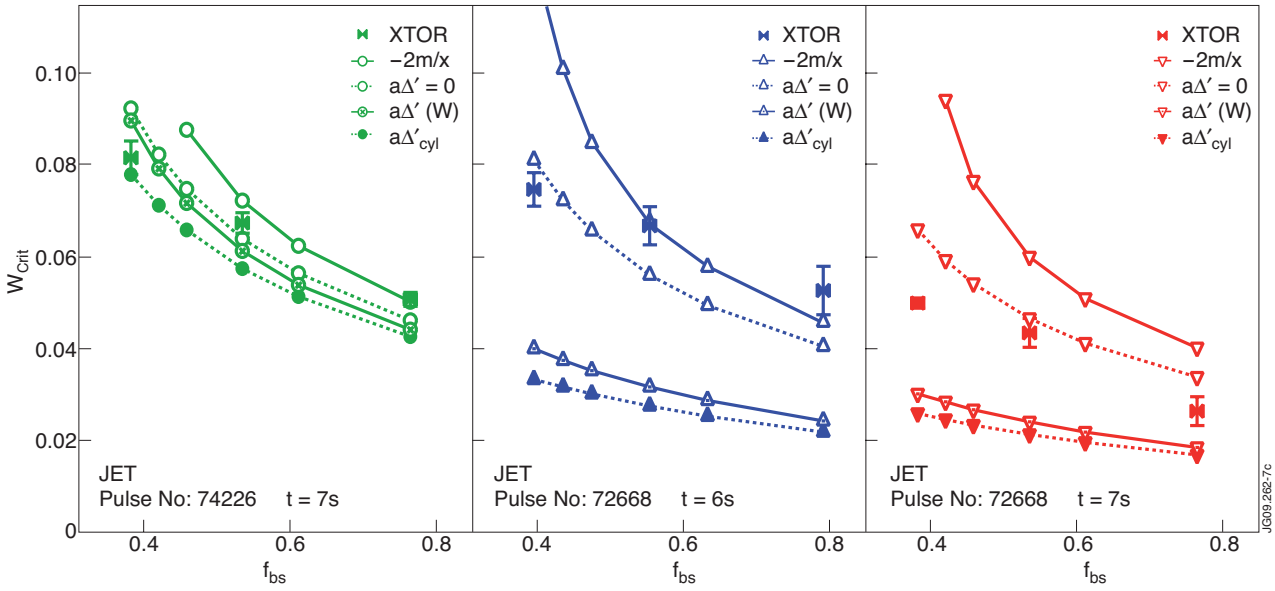

Figure 7: Critical island width as a function of the total bootstrap fraction, from XTOR and from the Generalized Rutherford Equation (equation 2) with different models for Δ′(W): $a\Delta' = -2m/x$, $a\Delta' = 0$, $a\Delta' = a\Delta'_{cyl.}$ and with the model $a\Delta'(W)$ of [40].

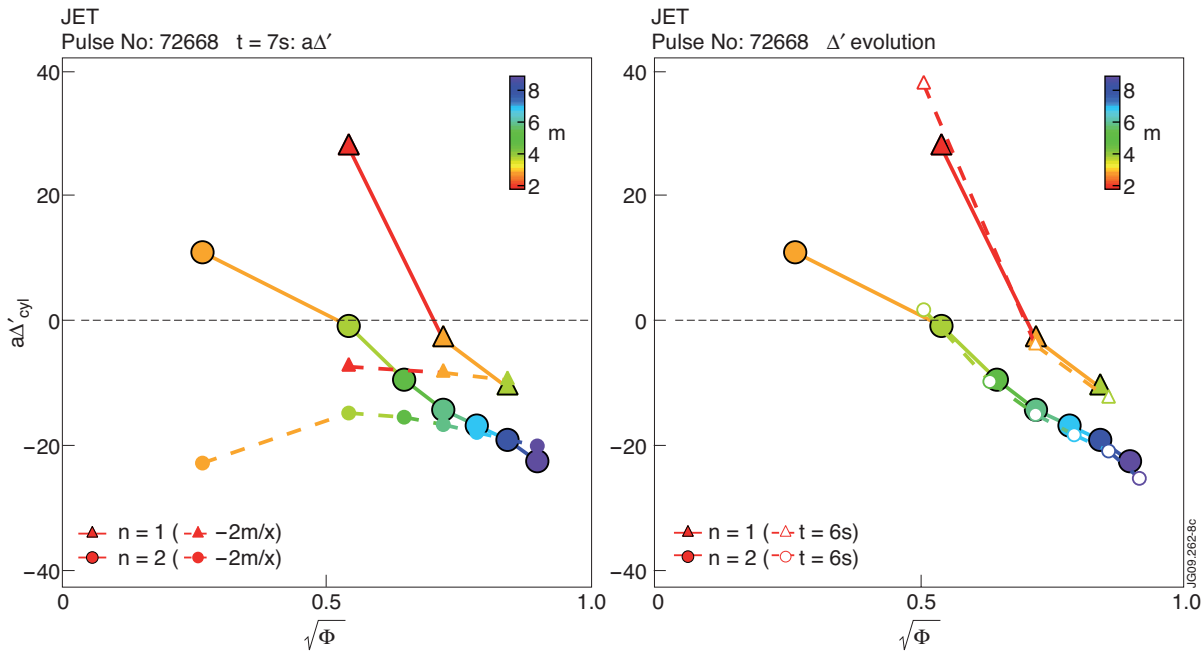

Figure 8: $a\Delta'_{cyl.}$ as a function of the radial position of resonant modes for Pulse No: 72668 case, compared to the simple evaluation $-2m/x$ (left); evolution between $t = 6s$ and $t = 7s$ (right). The color scale corresponds to the poloidal mode numbers.

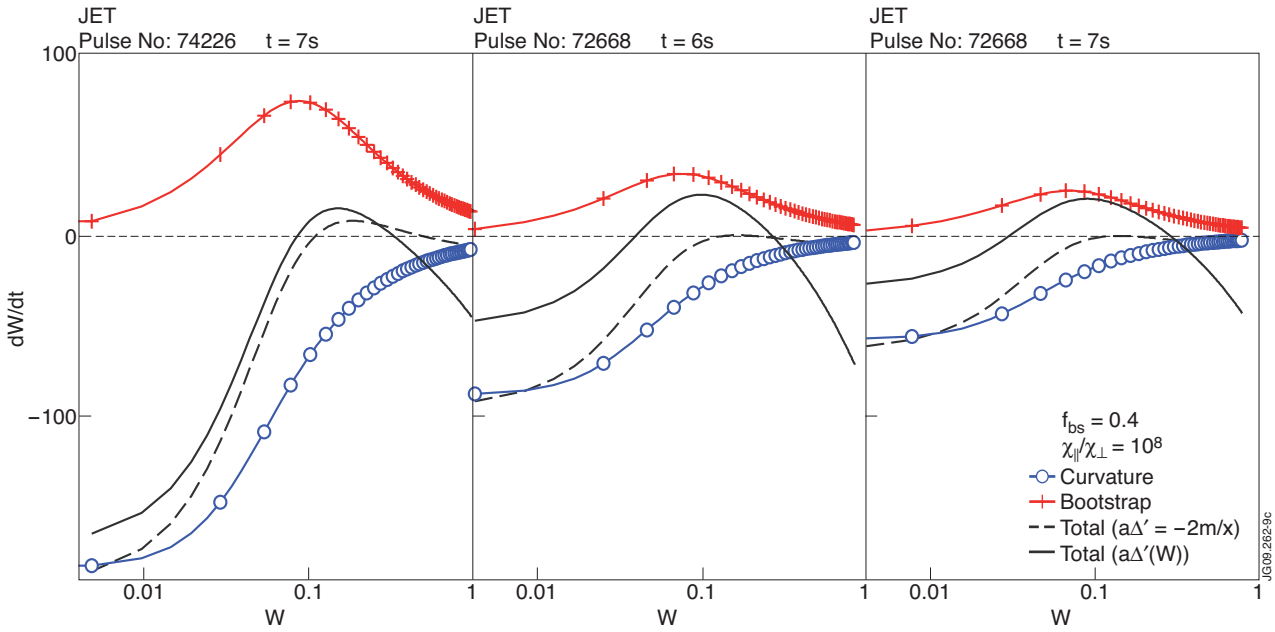

Figure 9. (dW/dt,W) diagram from Rutherford equation.

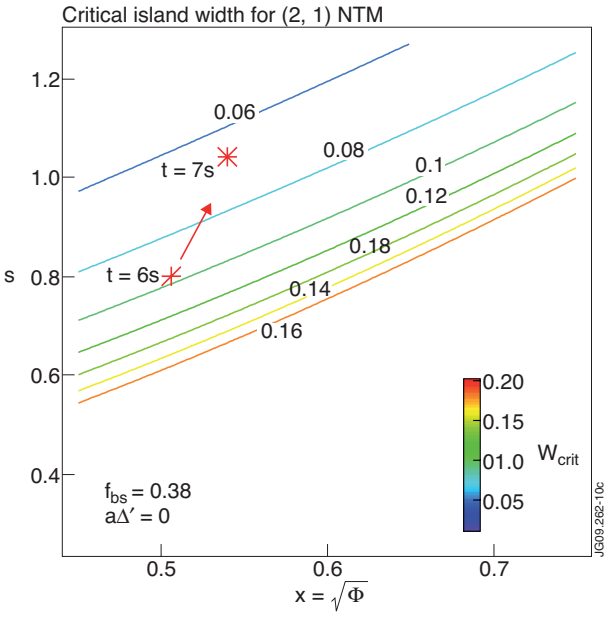

Figure 10. Effect of magnetic shear and position of q = 2 surface on critical island width, following Rutherford equation.

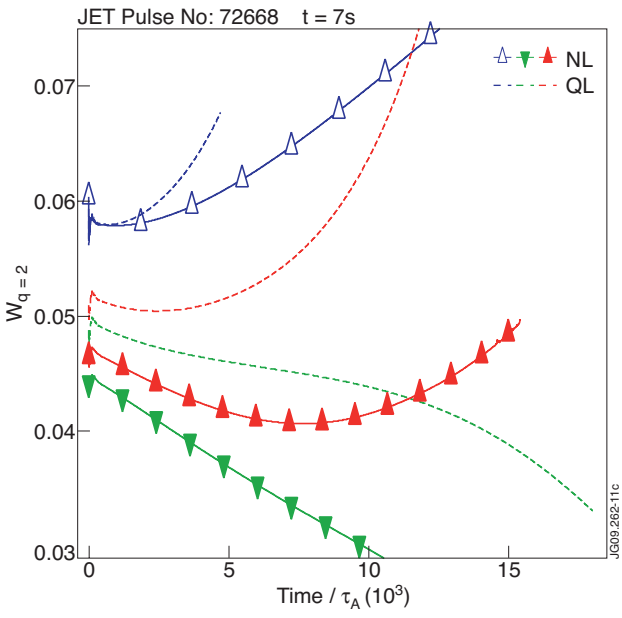

Figure 11: (2, 1) NTM evolution in Quasi-Linear (QL) and Non-Linear (NL) simulations.

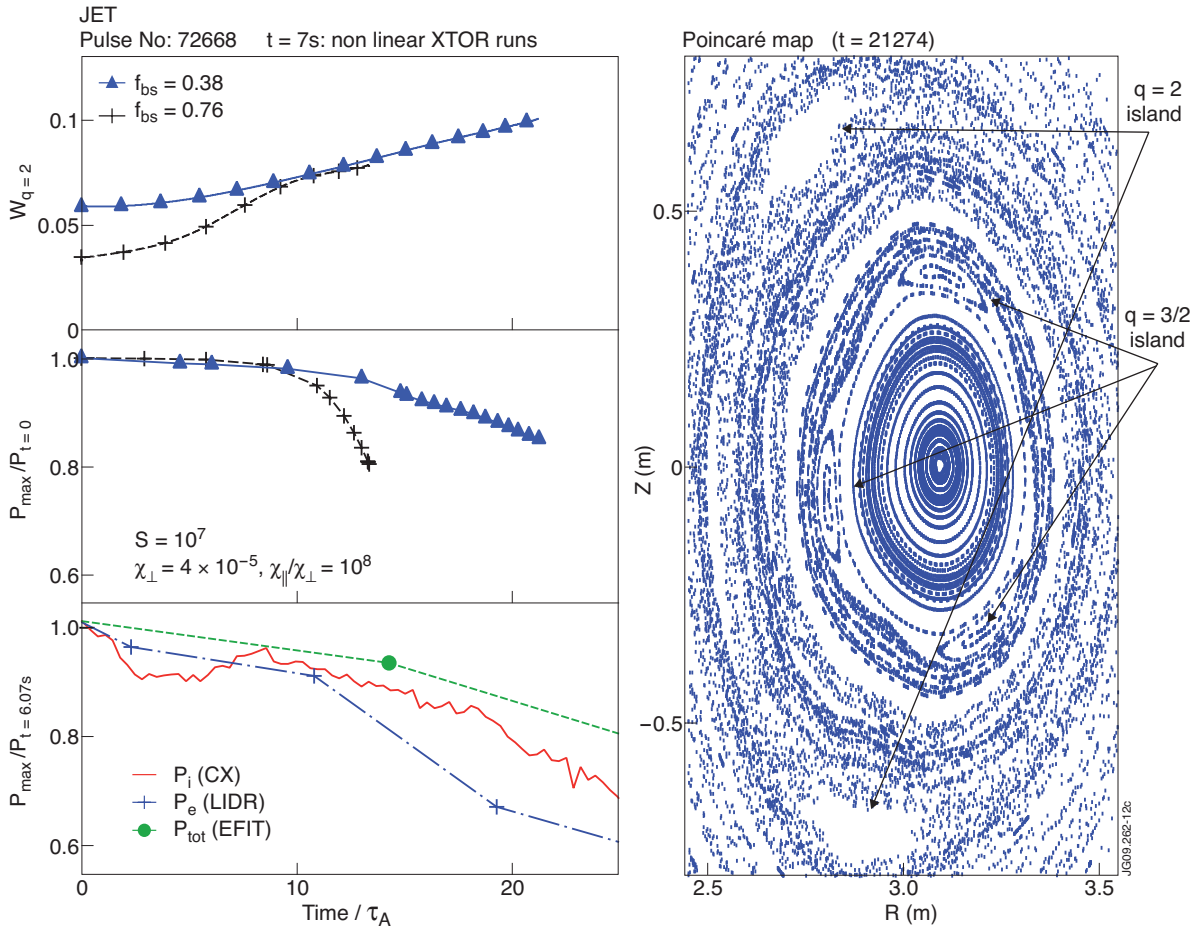

Figure 12: Non-Linear XTOR runs: q = 2 island size (top), maximum pressure (middle), and maximum ion, electron and total pressure from the experiment after rescaling the time (bottom). Right plot: Poincar´e map at the last simulation step (t = 21274 A).

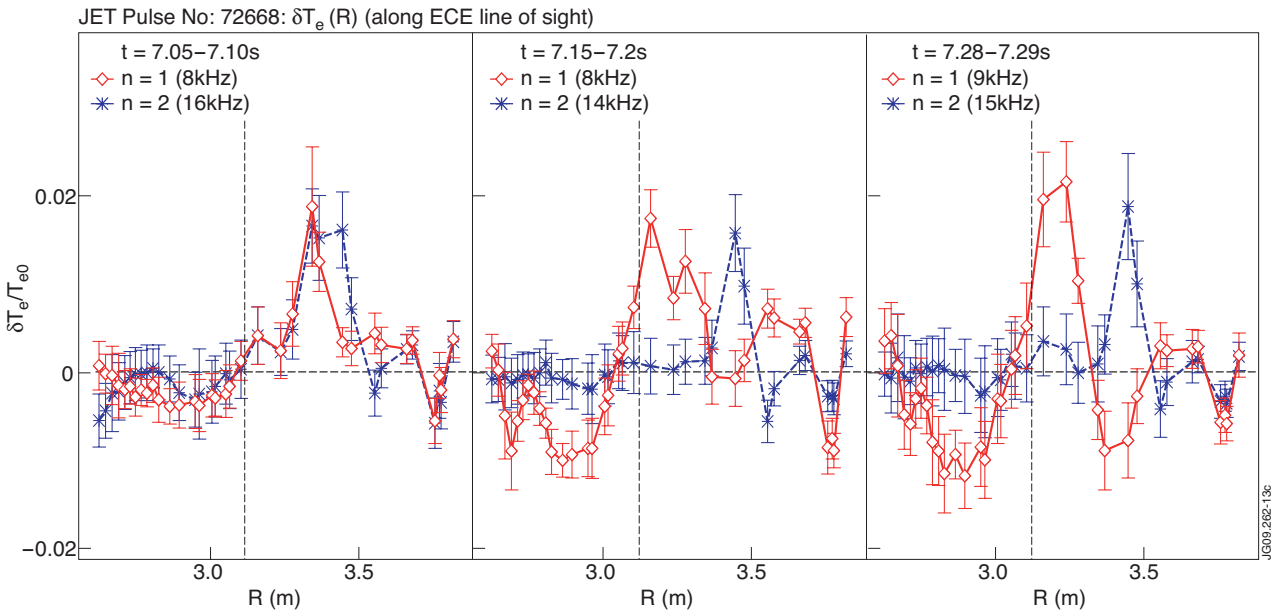

Figure 13: Evolution of n = 1 and n = 2 mode structures, as determined from the ECE diagnostic. The radial position of the magnetic axis from equilibrium reconstruction with EFIT is also indicated (note however that the magnetic axis is not on the line of sight of the diagnostic).

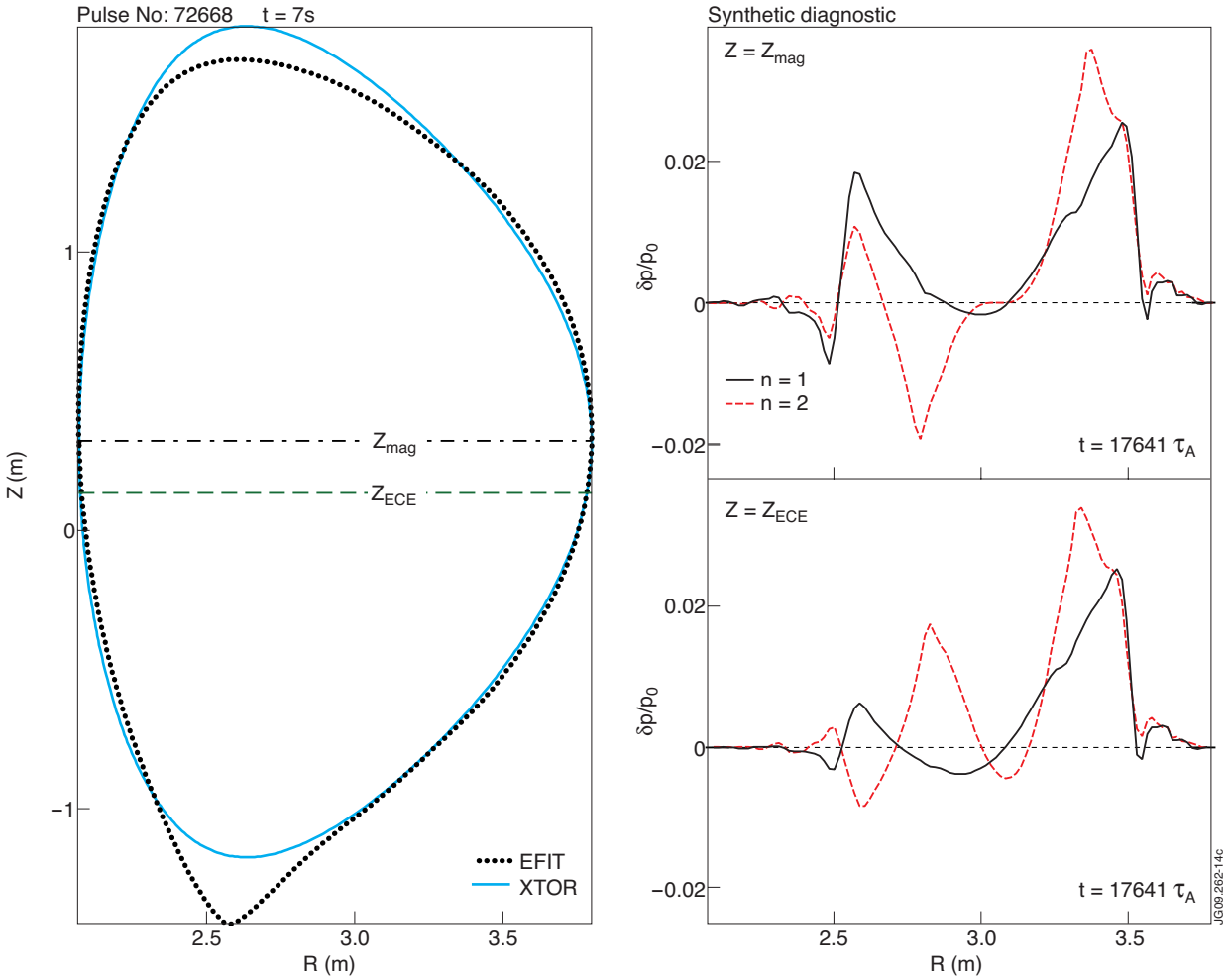

Figure 14: Magnetic equilibrium from EFIT and mean fit used in XTOR simulations for Pulse No: 72668 at t = 7s (left); mode structure deduced from the synthetic ECE diagnostic: δp at t = 17641 τ_A for a line of sight crossing the magnetic axis (top) and for the line of sight of the ECE radiometer in JET (bottom).

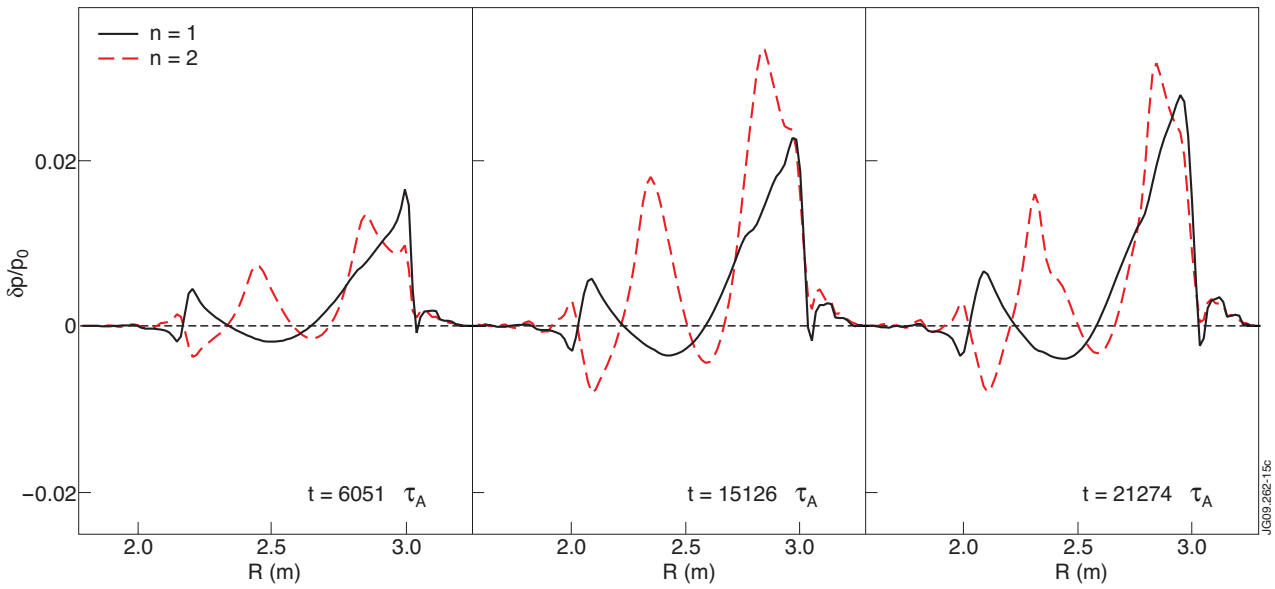

Figure 15: Mode structure deduced from δp at various times of the non linear simulation, with the line of sight of the ECE diagnostic.

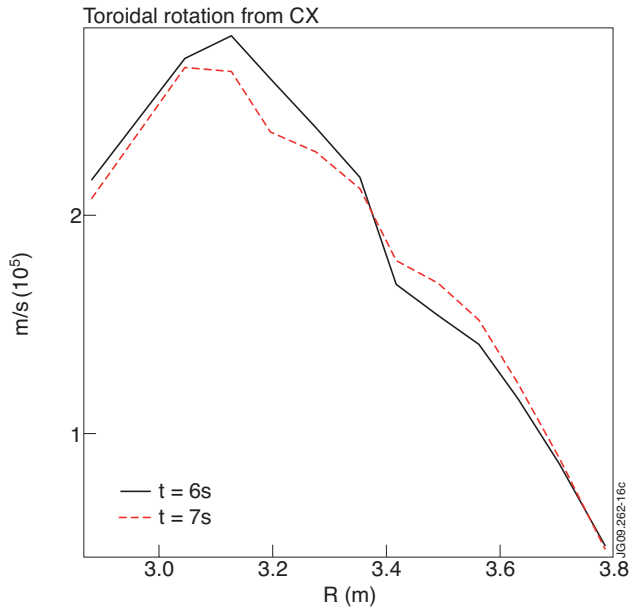

Figure 16. Toroidal rotation profile as measured by Charge Exchange diagnostic for Pulse No: 72668.